Articles

Preferential Forest Assembly of Single-Wall Carbon Nanotubes on Low-Energy Electron-Beam Patterned Nafion Films

Haoyan Wei,[‡] Sang Nyon Kim,[†] Harris L. Marcus,*[,‡] and Fotios Papadimitrakopoulos*[,†]

Department of Materials Science and Engineering, Institute of Materials Science, University of Connecticut, Storrs, Connecticut 06269, and Nanomaterials Optoelectronics Laboratory, Polymer Program, Institute of Materials Science, Department of Chemistry, University of Connecticut, Storrs, Connecticut 06269

Received May 19, 2005. Revised Manuscript Received November 29, 2005

With the aid of low-energy (500 eV) electron-beam direct writing, patterns of perpendicularly aligned single-wall carbon nanotube (SWNT) forests were realized on Nafion modified substrates via Fe^{3+}-assisted self-assembly. Infrared spectroscopy (IR), atomic force microscopy (AFM) profilometry, and contact angle measurements indicated that a low-energy electron beam cleaved the hydrophilic side chains ($-SO_3H$ and C−O−C) of Nafion to low-molecular-weight byproducts that sublimed in the ultrahigh vacuum (UHV) environment exposing the hydrophobic Nafion backbone. Auger mapping and AFM affirmed that the exposed hydrophobic domains absorbed considerably fewer Fe^{3+} ions upon exposure to pH 2.2 aqueous $FeCl_3$ solution, which yielded considerably less FeO(OH)/FeOCl precipitates (FeO(OH) in majority) upon washing with lightly basic DMF solution containing trace amounts of adsorbed moisture. Such differential deposition of FeO(OH)/FeOCl precipitates provided the basis for the patterned site-specific self-assembly of SWNT forests as demonstrated by AFM and resonance Raman spectroscopy.

1. Introduction

Single-wall and multiwall carbon nanotubes (SWNTs, MWNTs) have attracted considerable attention due to their unique structures, remarkable mechanical and electrical properties, and chemical stability.[1−4] SWNTs have found applicability in a wide range of electronics applications including nanodevices,[5−9] sensors,[10,11] and field emitters.[12,13] Their unique one-dimensional electronic structures make them ideal molecular wires to transport electrons from and to biological entities, such as peptides,[14−18] bound along their length or on their carboxylated ends[19] and therefore have received considerable attention in the design of nanoscale biosensors. The unique electron emission properties of vertically oriented nanotubes have attracted interest in the industry for flat panel displays,[13,20] parallel electron-beam nanolithography, and miniature X-ray generators.[21] For a number of these applications, it is very important to be able to produce uniform carbon nanotubes with controlled orientation normal to the substrates. In addition, to achieve

* To whom correspondence should be addressed. Phone: (860) 486-4623. Fax: (860) 486-4745. E-mail: hmarcus@mail.ims.uconn.edu (H.L.M.). Phone: (860) 486-3447. Fax: (860) 486-4745. E-mail: papadim@mail.ims.uconn.edu (F.P.).

[†] Nanomaterials Optoelectronics Laboratory.

[‡] Department of Materials Science and Engineering.

(1) Wildoer, J. W. G.; Venema, L. C.; Rinzler, A. G.; Smalley, R. E.; Dekker, C. *Nature* **1998**, *391*, 59.
(2) Odom, T. W.; Huang, J.-L.; Kim, P.; Lieber, C. M. *Nature* **1998**, *391*, 62.
(3) Dresselhaus, M. S.; Dresselhaus, G.; Eklund, P. C. *Science of Fullerences and Carbon Nanotubes*; Acadimic Press: San Diego, 1996.
(4) Yu, M.-F.; Files, B. S.; Arepalli, S.; Ruoff, R. S. *Phys. Rev. Lett.* **2000**, *84*, 5552.
(5) Bachtold, A.; Hadley, P.; Nakanishi, T.; Dekker, C. *Science* **2001**, *294*, 1317.
(6) Lefebvre, J.; Antonov, R. D.; Radosavljevic, M.; Lynch, J. F.; Llaguno, M.; Johnson, A. T. *Carbon* **2000**, *38*, 1745.
(7) Bockrath, M.; Cobden, D. H.; McEuen, P. L.; Chopra, N. G.; Zettl, A.; Thess, A.; Smalley, R. E. *Science* **1997**, *275*, 1922.
(8) Tans, S. J.; Devoret, M. H.; Dal, H.; Thess, A.; Smalley, R. E.; Geerligs, L. J.; Dekker, C. *Nature* **1997**, *386*, 474.
(9) Yao, Z.; Postma, H. W. C.; Balents, L.; Dekker, C. *Nature* **1999**, *402*, 273.
(10) Collins, P. G.; Bradley, K.; Ishigami, M.; Zettl, A. *Science* **2000**, *287*, 1801.
(11) Kong, J.; Franklin, N. R.; Zhou, C.; Chapline, M. G.; Peng, S.; Cho, K.; Dai, H. *Science* **2000**, *287*, 622.
(12) Lee, N. S.; Chung, D. S.; Han, I. T.; Kang, J. H.; Choi, Y. S.; Kim, H. Y.; Park, S. H.; Jin, Y. W.; Yi, W. K.; Yun, M. J.; Jung, J. E.; Lee, C. J.; You, J. H.; Jo, S. H.; Lee, C. G.; Kim, J. M. *Diamond Relat. Mater.* **2001**, *10*, 265.
(13) Oh, S. J.; Zhang, J.; Cheng, Y.; Shimoda, H.; Zhou, O. *Appl. Phys. Lett.* **2004**, *84*, 3738.
(14) Bahr, J. L.; Tour, J. M. *J. Mater. Chem.* **2002**, *12*, 1952.
(15) Yu, X.; Chattopadhyay, D.; Galeska, I.; Papadimitrakopoulos, F.; Rusling, J. F. *Electrochem. Commun.* **2003**, *5*, 408.
(16) Pantarotto, D.; Partidos, C. D.; Hoebeke, J.; Brown, F.; Kramer, E.; Briand, J.-P.; Muller, S.; Prato, M.; Bianco, A. *Chem. Biol.* **2003**, *10*, 961.
(17) Pantarotto, D.; Partidos, C. D.; Graff, R.; Hoebeke, J.; Briand, J.-P.; Prato, M.; Bianco, A. *J. Am. Chem. Soc.* **2003**, *125*, 6160.
(18) O'Connor, M.; Kim, S. N.; Killard, A. J.; Forster, R. J.; Smyth, M. R.; Papadimitrakopoulos, F.; Rusling, J. F. *Analyst* **2004**, *129*, 1176.
(19) Liu, J.; Rinzler, A. G.; Dai, H.; Hafner, J. H.; Bradley, R. K.; Boul, P. J.; Lu, A.; Iverson, T.; Shelimov, K.; Huffman, C. B.; Rodriguez-Macias, F.; Shon, Y.-S.; Lee, T. R.; Colbert, D. T.; Smalley, R. E. *Science* **1998**, *280*, 1253.
(20) Baughman, R. H.; Zakhidov, A. A.; de Heer, W. A. *Science* **2002**, *297*, 787.
(21) Sugie, H.; Tanemura, M.; Filip, V.; Iwata, K.; Takahashi, K.; Okuyama, F. *Appl. Phys. Lett.* **2001**, *78*, 2578.

10.1021/cm051074i CCC: $33.50
Published on Web 02/02/2006

point-source emission and localized electrochemical sensing, formation of spaced and laterally patterned SWNT probes with insulated side walls is also desired.[22] A number of researchers have reported on the growth of SWNTs and MWNTs using chemical vapor deposition (CVD) on patterned catalyst surfaces achieved via various methods such as standard lithography,[23,24] soft lithography,[25] ink-jet printing,[26] and nanochannel templates.[27,28] Although the CVD-grown carbon nanotubes possess the right orientation to serve as probes, they are loosely packed (density around 10^{11} cm^{-2}),[28] which renders them extremely difficult to handle in the presence of solvents, and upon drying they easily collapse. The coexistence of various types of SWNTs (metallic (met-) and semiconducting (sem-)) could also pose serious problems for electronic devices when only semiconducting or only metallic nanoprobes are needed.[20]

Prior research in our laboratory has shown that rope-lattice dense SWNT forests (density on the order of 10^{13} cm^{-2}) can be readily obtained by assembling nanotubes from dimethylformamide (DMF) dispersion onto an underlying Fe^{3+}/Nafion composite bed.[29] On the basis of this development, and the above concerns, we have directed our patterning efforts on self-assembled nanotube forests, which can also take advantage of postsynthesis SWNT separation according to length[30] and type (sem- versus met-).[31] Similar SWNT forest organization has been more recently reported using thiol functionalization of SWNT[32−34] as well as microcontact printing of SWNT dot arrays.[35] In contrast to Fe^{3+}-assisted forest assembly, these require longer adsorption times[33−35] and attain lower surface coverage.[32]

In the present contribution, we are reporting our initial findings in patterning these SWNT forests using low-energy electron-beam (500 eV) direct writing. The choice of low-energy electron-beam patterning was adopted for the following reasons: (1) The mean free path of low-energy electrons (10−500 eV) is small;[36] thus most of the energy will be deposited onto the top surface of polymer films.[37−39] In addition, the maximum interaction cross section (the probability of energetic electrons undergoing interaction with atoms) occurs at energy 2−3 times the binding energy for a specific element.[40] The larger the cross section, the better the chances of electron interaction with irradiated atoms. The electron beam used in this study (500 eV) is about 2 times the binding energy of carbon 1s (284.6 eV) and sulfur 2s (229.2 eV), and about 3 times the binding energy for sulfur 2p (164.05 eV), which provides the optimum interaction of electrons with Nafion films. (2) Present electron-beam lithography can still work very well in the nanoscale range at this voltage. (3) Below 1 keV is required to avoid electrical arcing in parallel electron column arrays which can increase the throughput substantially.[37] (4) Potential cross-contamination (carbonaceous impurities adsorbed onto Nafion/Fe^{3+} deposits) caused by chemical processing in traditional lithography can be prevented since no direct substrate contact is involved. We currently demonstrate that exposure of Nafion to a moderate dose (ca. 250−1250 $\mu C/cm^2$) of low-energy electrons (500 eV) causes a substantial loss of the hydrophilic side chains of Nafion in the immediate proximity of the surface of Nafion films, leaving behind a relatively hydrophobic surface, which impedes the absorption of Fe^{3+} ions and results in reduced assembly of SWNT forest arrays to the exposed regions.

2. Experimental Section

Nafion (5%) was purchased from Aldrich in water and lower aliphatic alcohols (1100 equivalent weight; i.e., 1100 g of polymer per mole of $-SO_3H$ groups). Iron(III) chloride hexahydrate ($FeCl_3 \cdot 6H_2O$, ACS reagent), nitric acid (70%), sulfuric acid (96.4%), and hydrochloric acid (38%) were also obtained from Aldrich and used as is. ACS reagent dimethylformamide (DMF) was purchased from J. T. Baker. Hydrogen peroxide (30%) and ACS certified methanol were obtained from Fisher Scientific. Millipore quality deionized water with resistivity larger than 18 MΩ was used for all experiments. Si(100) wafers were obtained from Montco Silicon and cleaned in Piranha solution (concentrated H_2SO_4 and 30% H_2O_2, 7:3 v/v) at 90 °C for 30 min. HiPco SWNTs were purchased from Carbon Nanotechnologies, Inc. Following the previously established protocol,[19,41,42] pristine SWNTs were treated in a 3:1 mixture of H_2SO_4 and HNO_3 with sonication for 4 h at 70 °C, filtered, washed with copious deionized water until the pH of filtrated water reached neutral, and dried overnight in a vacuum. Sonicating these purified shortened-SWNTs (s-SWNTs) in DMF resulted in a stable dispersion.

SWNT forests were fabricated using a procedure described previously.[29,43] Si substrates were first modified with Nafion via dipping in 1 mg/mL Nafion solution in methanol/H_2O (9:1 v/v) for 30 min to form a smooth and uniformly negatively charged surface. SWNT/Fe^{3+} assemblies were then obtained by sequential dipping of substrates in (i) $FeCl_3$ (pH 2.2, 15 min) solution, (ii) a

(22) Esplandiu, M. J.; Bittner, V. G.; Giapis, K. P.; Collier, C. P. *Nano Lett.* **2004**, *4*, 1717.
(23) Li, S. H.; Liu, H.; Li, H. F.; Zhai, J.; Jiang, L.; Zhu, D. B. *Synth. Met.* **2003**, *135*, 815.
(24) Wang, H.; Lin, J.; Huan, C. H. A.; Dong, P.; He, J.; Tang, S. H.; Eng, W. K.; Thong, T. L. J. *Appl. Surf. Sci.* **2001**, *181*, 248.
(25) Huang, L.; Wind, S. J.; O'Brien, S. P. *Nano Lett.* **2003**, *3*, 299.
(26) Ago, H.; Murata, K.; Yumura, M.; Yotani, J.; Uemura, S. *Appl. Phys. Lett.* **2003**, *82*, 811.
(27) Jeong, S. H.; Lee, K. H. *Synth. Met.* **2003**, *139*, 385.
(28) Li, J.; Papadopoulos, C.; Xu, J. M.; Moskovits, M. *Appl. Phys. Lett.* **1999**, *75*, 367.
(29) Chattopadhyay, D.; Galeska, I.; Papadimitrakopoulos, F. *J. Am. Chem. Soc.* **2001**, *123*, 9451.
(30) Chattopadhyay, D.; Lastella, S.; Kim, S.; Papadimitrakopoulos, F. *J. Am. Chem. Soc.* **2002**, *124*, 728.
(31) Chattopadhyay, D.; Galeska, I.; Papadimitrakopoulos, F. *J. Am. Chem. Soc.* **2003**, *125*, 3370.
(32) Liu, Z.; Shen, Z.; Zhu, T.; Hou, S.; Ying, L. *Langmuir* **2000**, *16*, 3569.
(33) Diao, P.; Liu, Z.; Wu, B.; Nan, X.; Zhang, J.; Wei, Z. *ChemPhysChem* **2002**, *3*, 898.
(34) Cai, L.; Bahr, J. L.; Yao, Y.; Tour, J. M. *Chem. Mater.* **2002**, *14*, 4235.
(35) Nan, X.; Gu, Z.; Liu, Z. *J. Colloid Interface Sci.* **2002**, *245*, 311.
(36) Geyer, W.; Stadler, V.; Eck, W.; Zharnikov, M.; Golzhauser, A.; Grunze, M. *Appl. Phys. Lett.* **1999**, *75*, 2401.
(37) Harnett, C. K.; Satyalakshmi, K. M.; Craighead, H. G. *Appl. Phys. Lett.* **2000**, *76*, 2466.
(38) Olkhovets, A.; Craighead, H. G. *J. Vac. Sci. Technol., B* **1999**, *17*, 1366.
(39) Seshadri, K.; Froyd, K.; Parikh, A. N.; Allara, D. L.; Lercel, M. J.; Craighead, H. G. *J. Phys. Chem.* **1996**, *100*, 15900.
(40) Rieke, P. C.; Baer, D. R.; Fryxell, G. E.; Engelhard, M. H.; Porter, M. S. *J. Vac. Sci. Technol., A* **1993**, *11*, 2292.
(41) Liu, J.; Casavant, M. J.; Cox, M.; Walters, D. A.; Boul, P.; Lu, W.; Rimberg, A. J.; Smith, K. A.; Colbert, D. T.; Smalley, R. E. *Chem. Phys. Lett.* **1999**, *303*, 125.
(42) Chattopadhyay, D.; Galeska, I.; Papadimitrakopoulos, F. *Carbon* **2002**, *40*, 985.
(43) Galeska, I.; Chattopadhyay, D.; Moussy, F.; Papadimitrakopoulos, F. *Biomacromolecules* **2000**, *1*, 202.

Scheme 1. Schematic Representation of the Formation of Patterned SWNT Forests

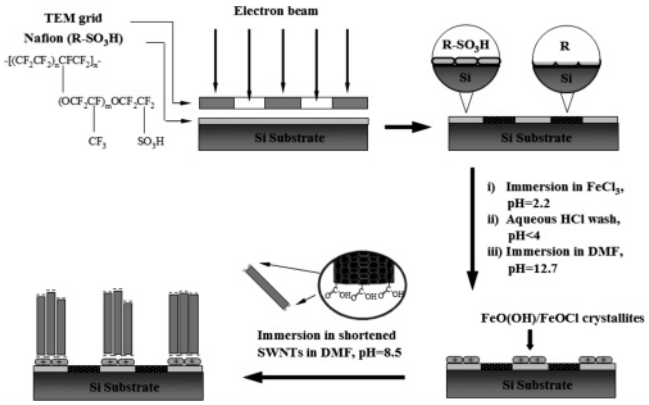

quick wash in aqueous HCl solution (pH <4) to remove loosely bound Fe^{3+} ions, (iii) a brief wash in DMF (pH 12.7) to remove excess water and facilitate Fe^{3+} ions to transform into their basic hydroxide form,[43] and (iv) a 30 min immersion in DMF dispersed SWNTs (pH 8.5) to enable the assembly of SWNT forest arrays.

Low-energy (500 eV) electron-beam patterning of Nafion modified Si substrates was performed in the PHI Auger 590 system with chamber pressure of $10^{-9}-10^{-10}$ Torr through a 500 mesh transmission electron microscope (TEM) copper grid blocking electrons from areas where the subsequent SWNT/Fe^{3+} deposition is desired (Scheme 1). A Faraday cup was used to measure the electron-beam current to calculate the doses for exposure. Infrared spectra (IR) samples were obtained on Nafion 112 membranes (50 μm thick, made from DuPont) with 2.5 × 3.5 mm irradiated rectangles at elevated accelerating voltage of 3 keV to obtain sufficient penetration depth for detection.

Atomic force microscopic (AFM) characterization was done on a Topometrix Explorer and Asylum Research MFP-3D in both contact mode and ac mode (tapping mode) to investigate the exposed Nafion films, iron deposits, and SWNT patterns. Liquid drop contact angle measurements on pristine and irradiated Nafion films were performed with water using the sessile drop mode (Ramé-Hart goniometer Model 100). IR attenuated total reflection (ATR) was done on a Spectra Tech IR-PLAN to study the possible irradiation mechanism on Nafion 112 membranes using a germanium (Ge) crystal with 1 μm probing depth. Spectra were collected before and after electron-beam irradiation and plotted without normalization. An X-ray photoelectron spectroscopic (XPS) survey of dipping acquired Nafion films was made on a Perkin-Elmer/PHI multiprobe surface analysis system with dual anode nonmonochromatic X-ray sources (PHI Model 04-548) operated at 15 keV and 250 W to produce Al X-rays. The multiprobe system was maintained at a base pressure of ca. 10^{-9} Torr. XPS data were collected at a pass energy of 89.45 eV. Controlled deposition of iron hydroxides was mapped in the same system by a PHI Auger 595 at 3 keV collecting elemental Fe LMM (atomic shells) at peak energy 598 eV. Morphology and crystallinity of iron deposits were investigated using a JEOL 2010 TEM operating at 200 keV accelerating voltage. Preferential self-assembly of SWNT forest was characterized by both AFM and Raman resonance spectroscopy using the AFM instruments mentioned above and a Renishaw Ramanscope 2000 equipped with a 785 nm laser source focused on a 1 μm spot by a 100× objective lens, respectively.

3. Results and Discussion

Depending on the dielectric constant (ϵ) of the organic solvent used for Nafion, the mixture can be categorized into three states: (1) solution ($\epsilon > 10$), (2) colloid ($3 < \epsilon < 10$), and (3) precipitates ($\epsilon < 3$).[44] Based on the solvent mixture (9/1 methanol/water) used in this study ($\epsilon > 38$), Nafion is in the form of clear solution in micellar conformation (hydrodynamic radius on the order of ca. 100 nm)[43] with most of its hydrophobic poly(tetrafluoroethylene) (PTFE) backbone buried inside and the hydrophilic sulfonate groups located outside of the micelle.[44] Upon immersion into the acidic Nafion solution (pH ~3), the partially protonated silanol groups (Si−OH) attracted the negatively charged Nafion micelles to deposit onto the Si substrate. This dipping process was shown to result in flattened or pancake-like Nafion assemblies with thickness on the order of 10 nm.[43] This rendered the top surface of this assembly extremely hydrophilic (contact angle < 10°). Successful deposition of Nafion film was further confirmed by Auger investigation as shown in Figure S1 in the Supporting Information. Nafion modified substrates were immediately transferred to an Auger system chamber for electron-beam patterning through a TEM grid (Scheme 1). Exposed Nafion samples were examined with AFM, both surface topology and friction force in contact mode (Figure 1); clear patterns were observed in both imaging modes. The topological depression of irradiated regions, as shown in Figure 1a,c, indicated that mass loss occurred during electron-beam exposure. Since Nafion irradiation was performed in an Auger chamber using the electron gun of the Auger spectrometer in standard configuration (i.e., pointing the sample at 45° instead of 90°) to pattern the Nafion film through a TEM grid, such irradiation configuration made it difficult to determine the precise height difference in AFM measurements as illustrated by the two orthogonal scans (Figure 1c), in which the measured values varied from 2 to 6 nm. Figure 1b gives the lateral force microscopic image which mapped surface chemical functionality.[45] Distinct friction-force differences were detected between electron-beam irradiated areas (squares) and unirradiated regions (grids), indicating an underlying transformation of Nafion's surface chemistry upon exposure to energetic electrons.

To obtain a better insight to Nafion's chemical transformation upon exposure to low-energy electron-beam irradiation, Fourier transform infrared (FTIR) ATR was utilized, which gives detailed information on the chemical functionalities. For our FTIR-ATR setup, Nafion film assembled according to the methodology described above produced insufficient signal-to-noise data and therefore we resorted to thicker Nafion membranes (ca. 50 μm). Since typical ATR detection depth is on the order of 1 μm, these thicker Nafion membranes were exposed to elevated beam voltage (3 keV) to increase the interaction depth with the electron beam. In Figure 2, the decreases of IR signal intensity for both SO_3^- symmetric stretching mode (peak centered at 1060 cm^{-1}) and C−O−C symmetric stretching mode (at 982 and 970 cm^{-1}) were observed for electron doses of 250 $\mu C/cm^2$ and above. This reduction of IR signal intensity for SO_3^- and C−O−C functionalities implied that Nafion's side chains (indicated by the dashed rectangle on Nafion's structures in

(44) Uchida, M.; Aoyama, Y.; Eda, N.; Ohta, A. *J. Electrochem. Soc.* **1995**, *142*, 463.
(45) Gardner, C. E.; Macpherson, J. V. *Anal. Chem.* **2002**, *74*, 576A.

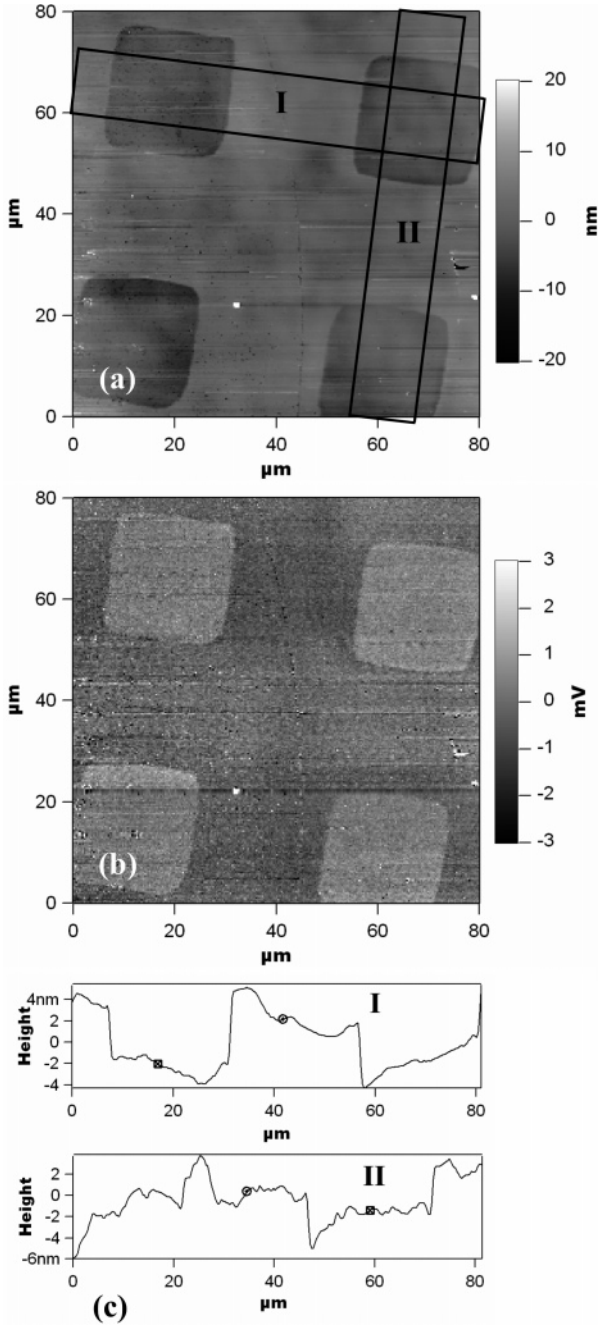

Figure 1. AFM images of grid-patterned Nafion irradiated with 500 eV electron-beam and dose of 750 μC/cm^2. Squares are the exposed regions. Topological (a) and lateral force microscopic (b) images. Topological profiles (c) along the indicated parallelograms in (a).

the inset of Figure 2) were susceptible to removal as a result of electron-beam irradiation[46] in high vacuum. We presently believe that for the irradiated section the majority of Nafion side chains located in the proximity of the surface were cleaved off and, due to their low molecular weight, these groups were sublimed to ultrahigh vacuum (10^{-9}−10^{-10} Torr). The scission of hydrophilic side chains, particularly the anionic SO_3^- groups, is expected to significantly reduce the ability of irradiated Nafion to absorb metal cations (i.e., Fe^{3+}). The fact that these three IR bands still maintained considerable intensity after electron-beam exposure to ir-

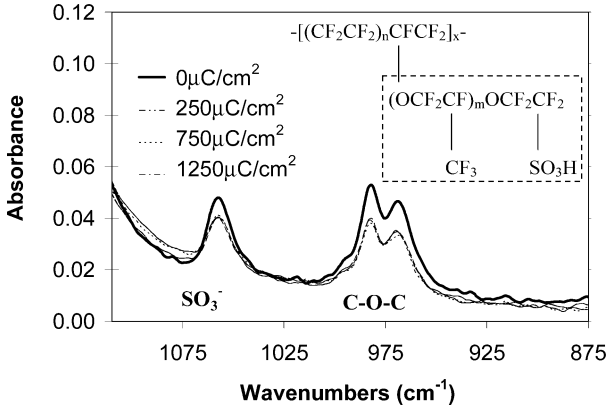

Figure 2. IR-ATR spectra of Nafion 112 membranes irradiated at 3 keV with different doses. Top right inset shows the chemical structure of Nafion with its hydrophilic side chain (indicated by the dashed rectangle) susceptible of removal upon electron-beam irradiation[46] in high vacuum.

radiation dosages as high as 1250 μC/cm^2 originates from the fact that the penetration depth of a 3 keV electron beam is much shallower (for reference, the electron range with the same energy for PMMA is around 200−300 nm[47]) than the probing depth of the ATR equipped with a Ge crystal (1 μm).

Hobson et al.[46,48,49] reported that upon electron-beam irradiation in the presence of oxygen (200 ppm oxygen under atmospheric conditions), the formation of carboxyl functionalities takes place at the sites of scission. This was witnessed by the emergence of the C═O stretch at 1770 cm^{-1}, which was assigned to the formation of carboxylic acid groups. As shown in Figure S2 of the Supporting Information, the formation of carboxyl impurities was avoided by the lack of a significant amount of oxygen in our system, which typically was operated at 10^{-9}−10^{-10} Torr. This absence of carboxylic acid groups was particularly important for our case in order to reduce Fe^{3+} absorption due to carboxylate salts in the irradiated Nafion areas.

The loss of sulfonate and other groups during irradiation was expected to render the surface less hydrophilic. This change was further supported by the contact angle measurements. Data are summarized as a function of electron doses in Figure 3, showing an apparent jump in the water contact angles in agreement with the FTIR results. Since wetting responses are believed to come from the very top surfaces (∼0.5 nm),[39] these increased contact angle values further confirmed the distinct changes in Nafion's surface chemistry.

The immersion of these electron beam patterned substrates into the $FeCl_3$ solutions caused differential absorption of Fe^{3+} ions according to SO_3^- content. Excessive $FeCl_3$ was removed from these substrates with an aqueous acidified (pH <4) wash before the samples were exposed onto a basic (pH 12.7) DMF wash. Residual surface water content as well as moisture impurities in DMF caused the adsorbed Fe^{3+} ions

(46) Hobson, L. J.; Ozu, H.; Yamaguchi, M.; Muramatsu, M.; Hayase, S. *J. Mater. Chem.* **2002**, *12*, 1650.
(47) Rai-Choudhury, P. *Handbook of Microlithography, Micromachining, and Microfabrication Volume 1: Microlithography*; SPIE Optical Engineering Press: Bellingham, WA; The Institution of Electrical Engineers: London, UK, 1997.
(48) Hobson, L. J.; Ozu, H.; Yamaguchi, M.; Hayase, S. *J. Electrochem. Soc.* **2001**, *148*, A1185.
(49) Hobson, L. J.; Oozu, H.; Yamaguchi, M.; Hayase, S. *J. New Mater. Electrochem. Syst.* **2002**, *5*, 113.

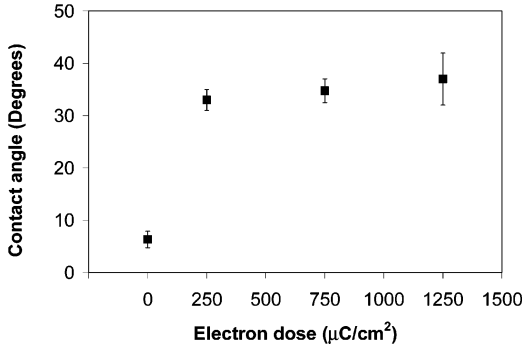

Figure 3. Contact angles of Nafion irradiated at 500 eV with different doses.

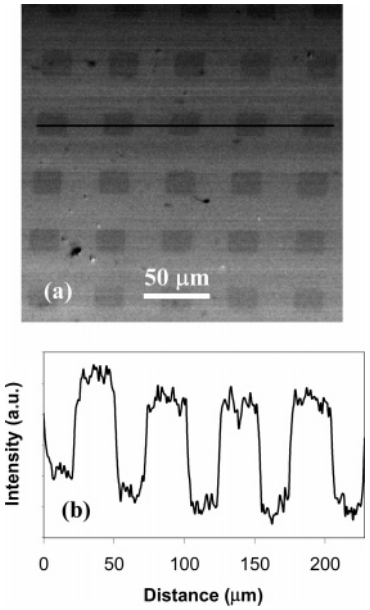

Figure 4. Typical Auger survey of iron deposits of grid-patterned Nafion at 500 eV with electron dose of 750 μC/cm^2. Squares are the exposed regions. Auger mapping of elemental Fe LMM at peak energy 598 eV (a). Corresponding line scan (see horizontal black line in (a)) of Fe as a function of distance (b).

to precipitate as hydroxides onto these patterned Nafion substrates. Figure 4a provides an iron LMM Auger elemental map collected at a peak of 598 eV. More iron was found in the brighter areas, which were those prevented from irradiation by the mask. Darker regions (squares) were iron-deficient due to the removal of the ionic groups of Nafion that were expected to strongly absorb Fe^{3+} ions. Figure 4b depicts the corresponding line scan at the same peak energy. Oscillation peaks due to the preferential distribution of iron concentration can be clearly observed. This selective metal functionalization is the key step to the formation of patterned SWNT forests.[29]

To determine the nature of these iron deposits, a TEM investigation (Figure 5) was performed. These precipitates appear to have crystalline morphology with size of ca. 100 nm in length and ca. 20 nm in diameter. Selected-area electron diffraction (SAED) investigation further revealed that these crystallites were mixtures of FeO(OH)/FeOCl (see Table S1 in Supporting Information). On the basis of the Fe/Cl ratio (>10) calculated from an Auger spectrum (Figure S3), it was deduced that the main component of these crystallites was FeO(OH). The fact that both adventitious carbon and Nafion contribute to the C signal in the Auger spectra and adventitious carbon could have different adsorption rates on irradiated and unirradiated surfaces makes it difficult to estimate the iron surface coverage by comparing the Fe/C peak ratios. The much higher C intensity in Figure S3b and peak shape similar to that in Figure S1 did indicate that part of the irradiated Nafion regions was exposed and devoid of iron deposits.

To compare quantitatively the deposition of FeO(OH)/FeOCl crystallites between exposed and unexposed areas, AFM topological imaging was performed. Figure 6a shows that the nonirradiation regions were fully covered with FeO(OH)/FeOCl crystallites forming continuous multilayers ($\geq$2). In contrast, in the electron beam exposed areas FeO(OH)/FeOCl existed as discrete crystallites in partial monolayer configuration. Image analysis software (ImageJ) was used to calculate the area fraction in Figure 6b by counting the image pixels, and the obtained surface coverage was ca. 42%. The root-mean-square (rms) surface roughness of these FeO(OH)/FeOCl deposits on the electron-beam unexposed regions, as measured by AFM, was found on the order of 10 nm (see Figure 7). Higher rms surface roughness values were observed for the irradiated regions, since FeO(OH)/FeOCl crystallites were separated from each other, resulting in a rougher surface topology. The plateau in Figure 7 indicates that a steady-state condition in FeO(OH)/FeOCl/Nafion roughness has been approached at exposure values similar to those observed from the IR investigation (Figure 2) and contact angle measurements (Figure 3). Much lower

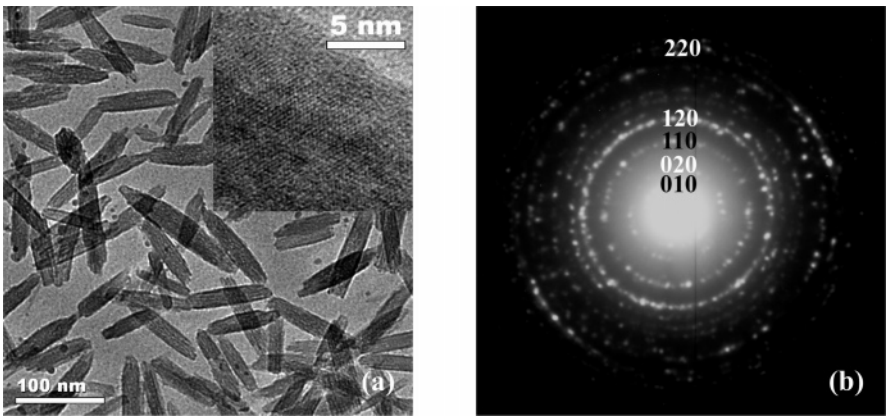

Figure 5. TEM bright field (BF) image (a) and diffraction patterns (b) of FeO(OH)/FeOCl precipitates. Inset in (a) shows a typical HRTEM lattice image of the crystalline FeO(OH)/FeOCl precipitates. White and dark *hkl* annotations in (b) correspond to the expected indices of FeO(OH) and FeOCl, respectively.

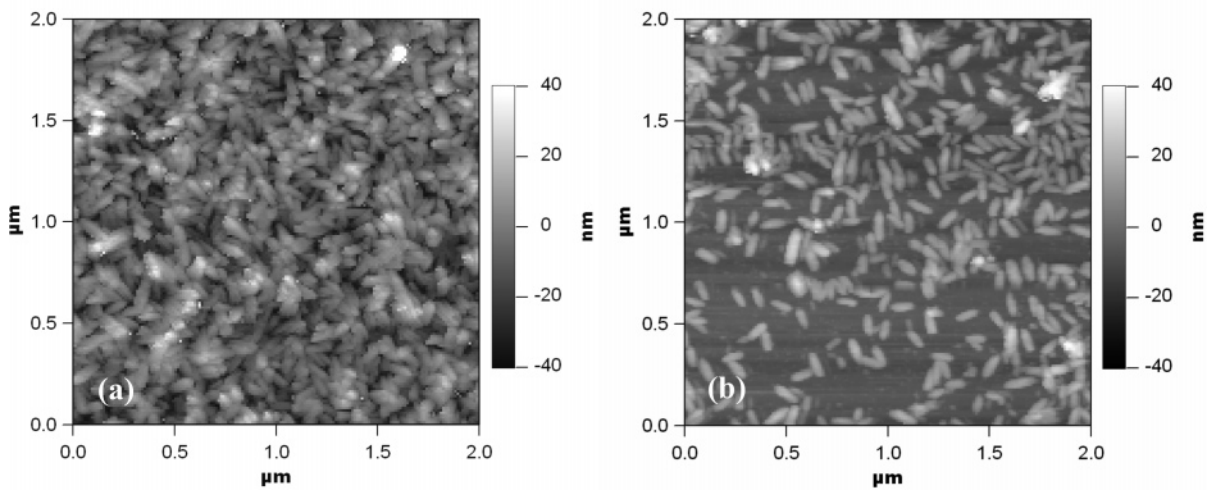

Figure 6. AFM images show FeO(OH)/FeOCl crystallites existing as continuous multilayers on nonirradiation regions (a) and in partial monolayer configuration on irradiation regions (500 eV, 750 μC/cm^2) (b).

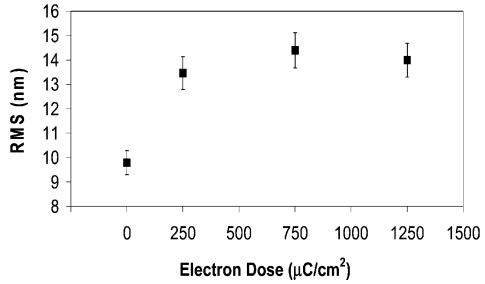

Figure 7. AFM measured surface roughness of FeO(OH)/FeOCl deposits on 500 eV electron beam exposed Nafion with different doses.

electron doses (50 and 150 μC/cm^2) were also tried, and the obtained patterns were not well-defined (data not shown).

Determining whether these FeO(OH)/FeOCl crystallites are on top of the exposed Nafion or underneath could prove important to better understand the subsequent forest self-organization of SWNTs onto irradiated Nafion regions. Contact angle measurements were assessed, but the small differences between irradiated (32° ± 2°) and unirradiated (27° ± 1°) regions were unable to provide a definite conclusion on the placement of these crystallites on the irradiated Nafion regions. The presence of strong Fe Auger signals (as shown in Figure S3 of the Supporting Information), however, suggested that these FeO(OH)/FeOCl crystallites were placed on top of the irradiated Nafion surface. Thus the question arises of where the Fe^{3+} ions are "stored" in these irradiated Nafion thin films and how they diffuse to the surface to form these FeO(OH)/FeOCl crystallites. The 4−8 nm thickness of the irradiated Nafion films certainly provides adequate porosity, and although after irradiation Nafion films become more hydrophobic (contact angle of 31−42°), it is still hydrophilic enough to ensure passage of Fe^{3+} ions. Figure S4 in the Supporting Information depicts the S 2p (164.40 eV) of thin Nafion films (ca. 10 nm thick) before and after irradiation (electron dose 1250 μC/cm^2). Although Nafion's low S content results in a signal-to-noise ratio far from ideal, we can safely conclude that complete SO_3^- elimination has not occurred and ca. 47% of sulfonate groups remain present as measured from the S peak areas in Figure S4. In addition, the underlying silanol groups (Si−OH) of the native silicon oxide layer is also capable of

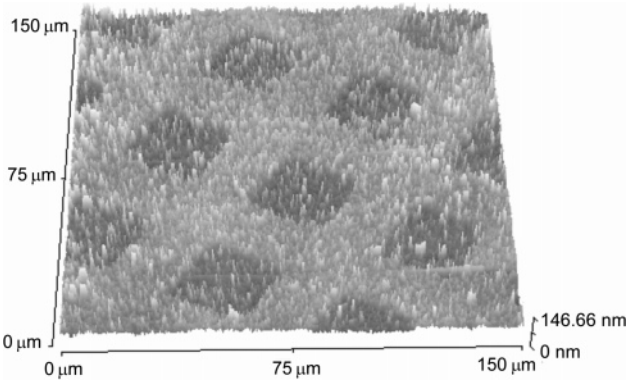

Figure 8. Representative AFM image of patterned SWNT forests. Nafion was patterned with 500 eV electron-beam irradiation (1250 μC/cm^2).

absorbing Fe^{3+} ions,[50−52] and their affinity to Fe^{3+} ions could be further enhanced upon electron-beam exposure, which we have confirmed by other experiments.[53] Upon washing in basic DMF (pH 12.7), Nafion could be plasticized by DMF, enabling Fe^{3+} to diffuse out. Residual water content in Nafion as well as moisture impurities in DMF would facilitate Fe^{3+} ions to transform into hydroxides. The Nafion/DMF boundary is the natural interface that the two reagents (Fe^{3+} and OH^-/H_2O) would meet and grow crystals of high order due to slow diffusion of both reagents from either side.

Upon immersion of these FeO(OH)/FeOCl decorated Nafion substrates into DMF dispersed shortened-SWNTs, acid−base neutralization between the carboxylic acid terminated nanotubes and the basic iron hydroxides provides the initial driving force for SWNT assembly.[29] The strong hydrophobic interaction between adjacent SWNT side walls is believed to further facilitate the bundling along the lateral direction, leading to rope-lattice SWNT forest assemblies. Figure 8 illustrates a typical AFM image of the resulting SWNT forests onto grid-patterned Nafion substrates. The majority of these forests were localized within the unexposed

(50) Mouche, F. T. L.; Derrien, J. *J. Electrochem. Soc.* **1995**, *142*, 2395.
(51) Okorn-Schmidt, H. F. *IBM J. Res. Dev.* **1999**, *43*, 351.
(52) Hattori, T. *Ultraclean Surface Processing of Silicon Wafers: Secrets of VLSI Manufacturing*; Springer-Verlag Telos: New York, 1998.
(53) Wei, H.; Kim, S.; Kim, S. N.; Marcus, H. L.; Papadimitrakopoulos, F. Manuscript in preparation.

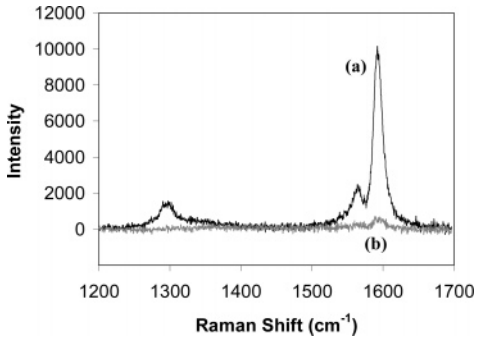

Figure 9. 785 nm Raman spectra of patterned SWNT forests taken at unexposed region (a) and exposed region (b), respectively. Nafion was patterned with 500 eV electron-beam irradiation (1250 μC/cm^2).

FeO(OH)/FeOCl regions, although some SWNTs still can be observed in the exposed region. Although the average length of DMF-dispersed s-SWNTs was 25−250 nm,[30] the average height of SWNT assemblies was on the order of 30−45 nm,[29] in agreement with prior reports.[18,33] Raman scattering provides further evidence for the preferential self-assembly of SWNT on patterned substrates, as shown in Figure 9 where in the nonirradiation regions a much higher signal intensity was observed at the characteristic G band (1592 cm^{-1}) than that in the exposed areas (peak height ratio $I_a/I_b = 24.6$). This ratio is significantly higher than that based on the FeO(OH)/FeOCl surface coverage between the unexposed and electron-beam-exposed regions, which was estimated to a ratio of ca. 2.4 according to AFM measurements. Since nanotube self-assembly is based on electrostatic ineractions[29] and such interactions extend from a few to tens of nanometers,[54] the positive polarity of the discrete FeO(OH)/FeOCl crystallites within exposed regions could be counteracted by the residual negative polarity of Nafion or Si substrates, thus reducing the electrostatic attraction of the negatively charged SWNTs. In contrast, fully covered multilayer FeO(OH)/FeOCl in the unexposed domains assured a clearly surface charge that attracted a significantly large number of SWNTs. Currently, efforts are underway to improve SWNT forest patterning, and these will be presented in subsequent publications.

(54) Bonnell, D. A. *Scanning probe microscopy and spectroscopy: theory, techniques, and applications*; Wiley-VCH: New York, 2001.

4. Conclusions

In this study we have demonstrated that a low-energy (500 eV) electron beam could sufficiently pattern Nafion and assist in selective localization of SWNT forests. During electron-beam exposure, a large number of sulfonate groups of Nafion were cleaved and removed in an ultrahigh vacuum, thereby reducing the ability of irradiated regions to withhold Fe^{3+} cations. Subsequent immersion into basic DMF solution resulted in the preferential deposition of iron hydroxides onto nonirradiation areas which was confirmed by Auger chemical mapping and AFM. This provided the basis for selective deposition of SWNTs into forest arrays as demonstrated by AFM and Raman spectra. These aligned and patterned SWNT forests could find a number of applications, such as field emission electron sources and biomaterial/nanotube hybrids for biosensor arrays.

Acknowledgment. The authors thank S. Kim for helpful discussion and assistance with liquid drop contact angle measurements, and R. Li for his help in the TEM experiments. The authors gratefully acknowledge the financial support of the U.S. Army Research Office (Grant ARO-DAAD-19-02-1-0381).

Supporting Information Available: Indexing table of FeO(OH)/FeOCl TEM diffraction pattern for Figure 5b (Table S1); Auger spectrum of dipping acquired Nafion films (Figure S1); IR-ATR spectra (1500−1900 cm^{-1}) of irradiated Nafion 112 membranes (Figure S2); Auger spectra of FeO(OH)/FeOCl crystallites on irradiated and unirradiated Nafion films (Figure S3); XPS investigation on S 2p of exposed and unexposed Nafion films (Figure S4) (PDF). This material is available free of charge via the Internet at http://pubs.acs.org.

CM051074I